The Astrophysical Journal, 621:725–737, 2005 March 10

KINEMATICS OF LOW-z ULTRALUMINOUS INFRARED GALAXIES AND IMPLICATIONS FOR DYNAMICAL MASS DERIVATIONS IN HIGH-z STAR-FORMING GALAXIES[1]

Luis Colina,[2] Santiago Arribas,[3,4] and A. Monreal-Ibero[5]

Received 2004 August 13; accepted 2004 November 15

ABSTRACT

The kinematic properties of the gaseous and stellar components of 11 ultraluminous infrared galaxies (ULIRGs; 14 nuclei) are investigated by means of integral field spectroscopy (IFS) with the INTEGRAL system and available IR and CO millimeter spectroscopy. The sample of ULIRGs cover different phases of the merging process and span all levels of activity from pure starbursts to Seyfert nuclei. The IFS data show that the ionized gas has a complex velocity structure with peak-to-peak velocity differences of a few to several hundred km s^{-1}, detected in tidal tails or extranuclear star-forming regions. The velocity field of the ionized gas on scales of a few to several kiloparsecs is dominated by tidally induced flows and does not, in general, correspond to rotationally supported systems with a privileged orientation along the major rotating axis. The central velocity amplitude of the ionized gas and stars shows discrepancies in some galaxies but has, on average, a similar value (ratio of 0.92 ± 0.37) , while the velocity amplitude of the molecular gas is a factor of 2 larger (ratio of 1.9 ± 0.6) than that of the stars and ionized gas. The central velocity amplitude measured using different kinematic tracers should therefore not be used in ULIRGs as a reliable tracer of mass, in general. The IFS data also show that the velocity dispersion of the ionized gas maps the large-scale motions associated with tidal tails and extranuclear regions, with often the highest velocity dispersion not being associated with the nucleus galaxies. There is, however, a good agreement between the central ionized gas and stellar velocity dispersions (ratio of 1.01 ± 0.13), while the cold molecular gas velocity dispersion has lower values (average of about 0.8 that of the stellar and ionized gas). The central ionized gas velocity dispersion is therefore a robust and homogeneous observable and a good tracer of the dynamical mass in these systems. The IFS-based central ionized gas velocity dispersion measurements confirm that ULIRGs' hosts are moderate-mass ($\leq m_*$) galaxies, as previously concluded by Tacconi and coworkers. In general, velocity amplitudes should not be used to estimate the dynamical mass in high-z star-forming systems, such as Lyman break and in particular submillimeter galaxies, since they show irregular stellar and gaseous structures similar to those present in low-z merging systems such as ULIRGs, the subject of this study. A more reliable method is to measure the central velocity dispersion using the strong, high equivalent width, rest-frame optical emission lines, provided the location of the nucleus is independently established by high angular resolution red or near-IR rest-frame imaging. The kinematics derived from the millimeter CO line suggest that the cold gas in ULIRGs does not share the velocity field of the stars and ionized gas and seems to be more rotationally supported. This result needs to be investigated in more detail with a larger sample of low-z ULIRGs before using the millimeter CO line widths as a dynamical mass tracer in high-z submillimeter galaxies.

Subject headings: galaxies: active — galaxies: interactions — galaxies: kinematics and dynamics — galaxies: nuclei — galaxies: starburst — infrared: galaxies

Online material: color figures

1. INTRODUCTION

Ultraluminous infrared galaxies (ULIRGs) are the most luminous objects in the local universe, with bolometric luminosities $L_{\rm bol} \approx L_{\rm IR} \geq 10^{12}\ L_\odot$. These galaxies are involved in strong interaction/merging processes traced by the presence of morphological peculiarities such as pairs of galaxies, galaxies with double nuclei, long tidal tails, or irregular stellar envelopes (see Bushouse et al. 2002; Farrah et al. 2001; Veilleux et al. 2002 and references therein). ULIRGs are also characterized as having large amounts of cold gas and dust in their nuclear regions (Solomon et al. 1997; J. Gracia et al. 2005, in preparation) and hosting an intense starburst activity that is the predominant source of energy in the majority of these galaxies (Lutz et al. 1998). Recent studies indicate that some, but not all, ULIRGs could evolve into QSOs (Colina et al. 2001; Tacconi et al. 2002). ULIRGs also seem to be systems that can transform gas-rich disk galaxies into moderate-mass (m_*) ellipticals through the process of merging (Genzel et al. 2001; Tacconi et al. 2002), therefore suggesting a physical mechanism for forming early-type galaxies in the early universe, such as those recently detected evolved stellar systems at redshifts of 2–3 (Franx et al. 2003; Cimatti et al. 2004; Förster-Schreiber et al. 2005; Van Dokkum et al. 2004).

[1] Based on observations with the William Herschel Telescope operated on the island of La Palma by the ING in the Spanish Observatorio del Roque de los Muchachos of the Instituto de Astrofísica de Canarias. Based also on observations with the NASA / ESA *Hubble Space Telescope*, obtained at the Space Telescope Science Institute, which is operated by the Association of Universities for Research in Astronomy, Inc., under NASA contract NAS5-26555.

[2] Instituto de Estructura de la Materia, Consejo Superior de Investigaciones Científicas (CSIC), Serrano 121, 28006 Madrid, Spain; colina@damir.iem.csic.es.

[3] Space Telescope Science Institute, 3700 San Martin Drive, Baltimore, MD; arribas@stsci.edu. Affiliated with the Space Telescope Division, Research and Science Support Department of ESA.

[4] On leave from the Instituto de Astrofísica de Canarias–Consejo Superior de Investigaciones Científicas (CSIC).

[5] Instituto de Astrofísica de Canarias, C/Via Láctea s/n, E-38205 La Laguna, Tenerife, Spain.

Deep submillimeter and radio surveys (Chapman et al. 2003a, 2003b, and references therein) are detecting a population of objects, the so-called submillimeter galaxies (SMGs), that appear to be forming stars at rates of up to 1000 $M_\odot$ yr^{-1} (i.e., up to 10 times more than ULIRGs) and that, according to their morphology (Chapman et al. 2003b), luminosity, and spectral energy distribution (Frayer et al. 2003; Egami et al. 2004), seem to be the high-z counterparts of the low-z luminous (LIRG) and ultraluminous (ULIRG) infrared galaxies (see Blain et al. 2002 for a review). The large quantities of internal dust and the cosmological dimming render the high-z SMGs largely undetected in the optical (rest-frame UV), except for the brightest sources (Chapman et al. 2003a) and those marginally detected in the near-IR. However, mid- and far-IR satellites (*Spitzer Space Telescope* and *Herschel*), as well as millimeter interferometers (IRAM, ALMA), continue to detect high-z LIRGs and ULIRGs in large quantities, as already shown by the first data taken with *Spitzer* (Charmandaris et al. 2004; Egami et al. 2004; Le Floch et al. 2004).

Studies of the evolution of the morphological types of galaxies as a function of redshift indicate that, as in low-z ULIRGs, mergers have played a major role in the shaping of present-day galaxies. These studies (Conselice et al. 2003, 2005; however, see Bell 2005) conclude that the fraction of galaxies consistent with undergoing a major merger increases with redshift for all galaxies, and at redshifts above 2, more than 80% of the stellar mass is in objects with peculiar morphology. There is also a predominance of irregular and complex morphologies in high-z luminous SMGs, suggesting that major mergers are common in these dusty star-forming galaxies (Chapman et al. 2003b). In addition, galaxies less affected by dust such as the Lyman-break galaxies (LBGs) and UV-selected, high-z star-forming galaxies often show irregular and distorted morphologies (Giavalisco et al. 1996; Erb et al. 2003, 2004), indicating that interaction/merging is also involved in these galaxies.

Although a good knowledge of the star formation history of the universe (Hopkins 2004) and the morphological evolution of galaxies (Conselice et al. 2003, 2005) is starting to emerge, the knowledge of another fundamental quantity, the mass assembly of galaxies over cosmic time, is comparatively very poor. The evolution of the stellar mass distribution over cosmic time is beginning to be investigated up to a redshift of 3 using deep optical and near-IR imaging of small portions of the sky and spectral energy distribution modeling (Dickinson et al. 2003; Conselice et al. 2005; Barmby et al. 2004) or studies of LBGs (Papovich et al. 2001; Shapley et al. 2001; Barmby et al. 2004). Dynamical mass measurements are even more scarce and limited thus far to small samples of LBGs (Pettini et al. 2001; Erb et al. 2003, 2004), and a few SMGs (Genzel et al. 2003; Neri et al. 2003) for which near-IR long-slit or millimeter wave interferometry observations are becoming available.

As for the samples of luminous LBGs and SMGs already being investigated, the future measurements of dynamical masses in less luminous, high-z galaxies will also involve subarcsecond near- and mid-IR imaging and spectroscopy (*James Webb Space Telescope* [*JWST*] and large ground-based telescopes) or millimeter interferometer spectroscopy (ALMA). The dynamical mass will be derived from the kinematics of the warm, ionized gas (traced by optical emission lines like Hα), cold molecular gas (traced by millimeter CO lines in emission), or even the stars (traced by near-IR absorption lines such as CaT or CO bandhead). The use of one or more of these techniques will depend very much on the type of galaxy, and the combination of all of them would be used to probe the dynamical mass distribution in representative samples of different high-z objects. As strong interactions and mergers are common in the high-z universe, it is worth investigating the agreement and reliability of the different kinematic observables used to trace dynamical mass in a sample of low-z mergers, such as the ULIRGs presented in this paper, for most of which the required data, near-IR imaging, integral field optical spectroscopy, near-IR long-slit spectroscopy, and millimeter interferometer maps are available.

The paper is organized as follows. Section 2 presents the sample of ULIRGs and explains the pedigree of the different data used in this work. Section 3 summarizes the kinematics, velocity field, and velocity dispersion of the ionized gas as derived from optical integral field spectroscopy (IFS) with the INTEGRAL system. These results are then compared with those obtained using other techniques such as near-IR and millimeter spectroscopy. Section 4 discusses the velocity dispersion used to estimate the dynamical mass, the reliability of the method, and the implications for dynamical mass estimates in high-z galaxies.

2. THE SAMPLE OF ULIRGs: GENERAL PROPERTIES AND KINEMATIC DATA

Since the goal of this investigation is the comparison of different observables used as dynamical mass tracers in low-z ULIRGs, the galaxies in the sample were selected by having at least two different tracers (optical emission lines such as Hα, near-IR CO absorption bands, or millimeter CO emission line) measured with similar spatial resolution, already available. The Hα measurements come from an ongoing IFS survey of ULIRGs to probe the internal structure and kinematic properties of the extended ionized gas using INTEGRAL, a fiber-fed integral field system mounted on the 4.2 m William Herschel telescope (Arribas et al. 1998). The near-IR measurements were taken as part of a survey of ULIRGs to investigate their stellar kinematic properties using long-slit spectroscopy on the VLT and Keck telescopes (Genzel et al. 2001; Tacconi et al. 2002). Finally, the CO millimeter measurements, providing information on the kinematics of the cold molecular gas, were taken with the Plateau de Bure or Owens Valley interferometers (Downes & Solomon 1998; Evans et al. 2002), except for IRAS 15206+3342 and IRAS 20087−0308, for which single-dish measurements were used in this study. The angular resolution varies slightly between these different set of data. While near-IR measurements are obtained with a 0.″6 slit (Genzel et al. 2001), the integral field data have resolution elements (fibers) of 0.″9 in diameter (Arribas & Colina 2003). Millimeter observations were obtained with FWHM resolutions of 0.″5–1.″0 and $\sim$2.″6 × 1.″9 for the Plateau de Bure (Downes & Solomon 1998), and Owens Valley (Evans et al. 2002) interferometers, respectively. For the range of distances covered by the sample, 1″ angular resolution represents, on average, a linear size of 1.3 kpc, ranging from 0.4 kpc (Arp 220) to 2.6 kpc (IRAS 15206+3342). On the other hand, the spectral (i.e., velocity) resolution varies from the low resolution (R = 1500) of the IFS to the intermediate values (R = 2200–5200) of the near-IR long-slit spectroscopy and the high resolution (R = 7500–15,000) of the Plateau de Bure millimeter data. The instrument velocity resolution of these data (equivalent to $\sigma_{\rm instr} \leq 85$ km s^{-1}) is enough to resolve the profiles of the different emission and absorption lines in these systems.

The entire sample consists of 11 ULIRGs with a total of 14 nuclei, since three of the ULIRGs (IRAS 08572+3915, IRAS 12112+0305, and IRAS 14348−1447) are interacting pairs separated by several seconds of arc and well-resolved nuclei. A subsample of eight ULIRGs, including the three double-nucleus systems, have IFS taken as part of our ongoing program. The

TABLE 1
ULIRG Sample: General Properties

Galaxy	Redshift[a]	$\log L_{IR}$[b] ($L_\odot$)	Activity[c]	IR Class[d]	Morphology[e]
IRAS 08572+3915	0.05835	12.15	H II/LI	W	Interacting pair at 6.0 kpc
Mrk 231	0.04217	12.55	S1	W	Single nucleus
Mrk 273	0.03778	12.16	S2/LI	C	Double nucleus at 0.78 kpc
IRAS 12112+0305	0.07332	12.35	LI	C	Interacting pair at 4.5 kpc
IRAS 14348-1447	0.08273	12.37	LI	C	Interacting pair at 6.2 kpc
IRAS 15206+3342	0.12441	12.25	LI/H II	W/C	Single nucleus
IRAS 15250+3609	0.05516	12.07	LI	C	Single nucleus
Arp 220	0.01813	12.17	H II	C	Double nucleus at 0.36 kpc
IRAS 17208-0014	0.04281	12.41	LI	C	Single nucleus
IRAS 20087-0308	0.10567	12.46	S2	C	Single nucleus
IRAS 23365+3604	0.06448	12.18	LI	C	Single nucleus

[a] Redshifts taken from the NASA/IPAC Extragalactic Database (NED).
[b] Luminosities calculated using the L_{IR} expression given in Sanders & Mirabel (1996), and a distance luminosity assuming $\Omega_M = 0.3$, $\Omega_\Lambda = 0.7$, and H_0 of 70 km s^{-1} Mpc^{-1}.
[c] Classification based on optical emission-line ratios (S1: Seyfert 1; S2: Seyfert 2; LI: LINER; H II: H II region). More than one class for the same galaxy indicates different classification in the literature.
[d] IR class according to the standard classification by which warm (W) ULIRGs have $f_{25}/f_{60} > 0.2$, while cool (C) ULIRGs have $f_{25}/f_{60} \leq 0.2$.
[e] Morphology derived from high spatial resolution *HST* WFPC2 or NICMOS imaging.

entire sample, albeit small in size, is representative of ULIRGs, covering a wide range of morphologies representing different phases of the merging process from well-separated interacting pairs (i.e., IRAS 08572+3915, IRAS 12112+0305) to double-nucleus galaxies (angular separation less than 1″, i.e., Arp 220, Mrk 273), and single, QSO-like nuclei (i.e., Mrk 231). Also, the full range of nuclear activity from H II and LINERs to Seyfert 1 and 2 galaxies is covered. Finally, as defined by the ratio of the 25 and 60 μm IRAS bands, both warm ($f_{25}/f_{60} \geq 0.2$) and cool ($f_{25}/f_{60} < 0.2$) ULIRGs are included in the sample. General properties of each of the galaxies are listed in Table 1.

3. RESULTS

The results of the subsample of ULIRGs for which integral field optical spectroscopy with the INTEGRAL system is available are presented in Figure 1 and summarized in Table 2. In the following sections, a detailed discussion of the spatial distribution and kinematics (velocity field and velocity dispersion maps) of the ionized gas based on these results is given. Throughout the rest of the paper, the kinematic major axis refers to the line defining the largest velocity amplitude within the inner ±2″.0 around the nucleus. For those ULIRGs where two galaxies with their stellar nuclei are still clearly identified (i.e., interacting pairs like IRAS 08572+3915, IRAS 12112+0305, and IRAS 14348−1447), the photometric major axis of the system is considered to be the line joining the two nuclei.

3.1. *Comments on Individual Objects*

The salient morphological and kinematical features of the ionized gas presented in Figure 1 for each of the galaxies observed with INTEGRAL are summarized in this section. All mentioned velocities and distances correspond to observed values and therefore have not been corrected for any projection effects. Detailed IFS studies of several galaxies have already been presented elsewhere and are cited in the text for additional information.

IRAS 08572+3915.—This is one of the interacting pairs in the sample having two stellar nuclei separated by 6 kpc. The Hα emission is dominated by two regions associated with the stellar nuclei of the system. The velocity dispersion map indicates that the north component is the more massive galaxy in this system. Although the large-scale structure of the velocity field is not consistent with rotation, the small-scale velocity pattern around the two nuclei could be consistent with it (Arribas et al. 2000). Additional higher angular resolution data are needed to support this claim.

Mrk 273.—This is a double-nucleus galaxy with the two nuclei at a distance of 0.8 kpc. The optical and near-IR continuum light show the same distribution elongated along the north-south direction. The Hα emission shows the emission peak associated with the nucleus and an extended, lower surface brightness region at distances of about 3 kpc along the position angle (P.A.) 240 (Colina et al. 1999). The velocity dispersion and velocity field cover a small range in velocities without any indications of strong spatial and kinematical substructure.

IRAS 12112+0305.—This is an interacting pair with galaxies at a projected distance of 4.5 kpc. The Hα light identifies the brightest near-IR nucleus as a weak Hα source, due to differential extinction toward the nucleus (Colina et al. 2000). The Hα emission is dominated by an extranuclear star-forming region located at 7.5 kpc east-northeast of the near-IR nucleus and by the secondary near-IR nucleus and associated tail (Colina et al. 2000). The peak in velocity dispersion does not correspond to any of the two near-IR nuclei (i.e., stellar nuclei) but with a region north of the secondary nucleus. The velocity field also shows a complex velocity structure with the northwest tail receding with a velocity of −300 km s^{-1} relative to the system. These kinematical features indicates that this ULIRG is a dynamically young system.

IRAS 14348−1447.—This is an nteracting pair of galaxies separated by 6.2 kpc. The Hα light is dominated by the emission from the brightest (southern) nucleus. The secondary peak in the Hα light distribution does not correspond to the second (northern) nucleus, which is a weak source, but rather with star-forming knots located in the inner regions of the tidal tail, at a distance of 3.6 kpc away from the northern nucleus. A third, weak Hα emission peak is located at 9.3 kpc southeast from the southern nucleus, and it is associated with an extranuclear, extended region identified in *Hubble Space Telescope* (*HST*) optical images (Monreal 2004). While the velocity dispersion peak spatially coincides with the southern nucleus, the amplitude of

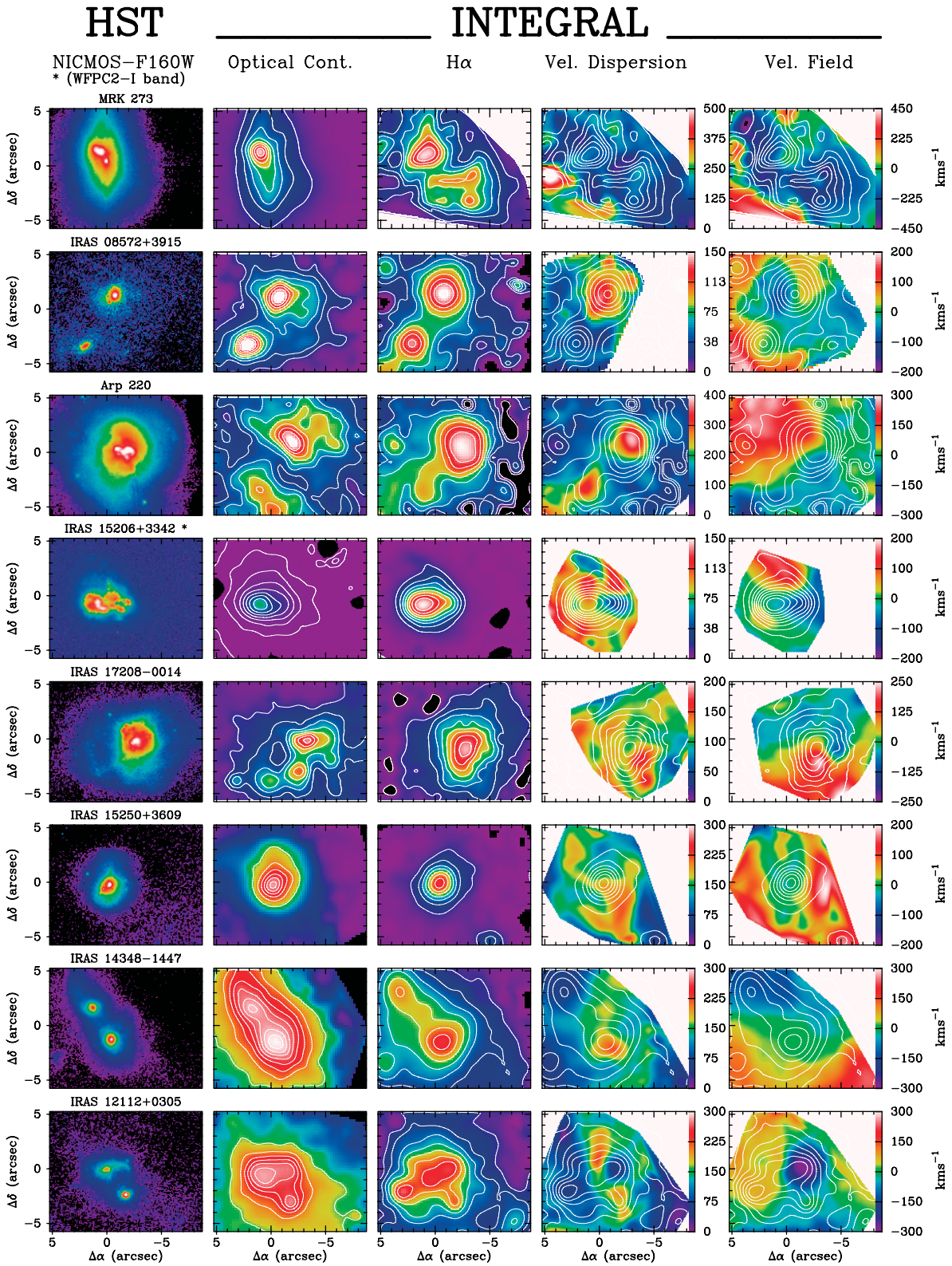

FIG. 1.—Results for the eight ULIRGs with available IFS. The stellar and ionized gas distribution are traced by the optical continuum (*second column from the left*), and Hα line (*center column*). The kinematic properties of the ionized gas are represented by the velocity dispersion map (*second column from the right*) and the velocity field (*right column*). The optical continuum and the Hα images have superposed linearly scaled isocontours. The Hα contours are superposed on the velocity dispersion and velocity field maps. The near-IR (NICMOS F160W filter) *HST* imaging is also shown on the left side for comparison. Note that position (0, 0) does not correspond to the adopted nucleus of the systems but to an arbitrary position within each field.

TABLE 2
INTEGRAL FIELD ULIRG SUBSAMPLE: STELLAR VERSUS IONIZED GAS CHARACTERISTICS

Galaxy	Scale (kpc/arcsec)	$N_{stellar}$[a]	$N_{stellar\text{-}gas}$[b]	Rotation[c]	$Axis_{stellar\text{-}gas}$[d] (deg)	$Mass_{stellar\text{-}gas}$[e]
IRAS 08572+3915 NW.....	1.2	Yes	Yes	Yes?	<45	Yes
IRAS 08572+3915 SE.....	1.2	Yes	Yes	Yes?	~0	No
Mrk 273	0.8	Yes	Yes	No	~90	No
IRAS 12112+0305 NE	1.5	Yes	No	No	~90	No
IRAS 12112+0305 SW.....	1.5	Yes	No	No	...	Yes
IRAS 14348-1447 NE	1.7	Yes	No	Yes?	~90	No
IRAS 14348-1447 SW.....	1.7	Yes	Yes	No	≤45	Yes
IRAS 15206+3342.....	2.6	Yes	Yes	No?	~45	No
IRAS 15250+3609.....	1.1	Yes	Yes	No	...	No
Arp 220.....	0.4	No	No	Yes	~90	Yes
IRAS 17208-0014.....	0.9	No	No	Yes	~0	Yes

[a] This column indicates whether the optical and near-IR nucleus (identified by the peak emission in their light distribution) have the same position, i.e., spatially coincident within ±0.″5.

[b] This column indicates whether or not the peak of the ionized gas distribution (as traced by the Hα emission line) and the stellar nucleus (traced by the *H*-band light) have the same position, i.e. spatially coincident within ±0.″5.

[c] This column indicates whether or not the gas velocity field obtained from the measurements of the Hα emission line is compatible with rotation. Velocity fields consistent with regular radial velocity gradients within ±2″ of the nucleus are identified as possible candidates for rotation ("yes?" in fifth column).

[d] Angular difference between the photometric major axis, defined as the predominant direction of the light distribution (in interacting pairs line along the two nuclei) and the direction of largest velocity amplitude at distances of ±2″. In systems with two nuclei, the line joining the nuclei is considered as the photometric axis. IRAS 12112+0305 SW and IRAS 15250+3609 do not show any measurable velocity gradient within ±2.

[e] This column indicates whether the peak of the stellar mass distribution traced by the *H*-band light coincides with the peak of the dynamical mass, traced by the Hα velocity dispersion.

the velocity field is small (less than 150 km s^{-1}) in the central regions and does not show evidence for rotation around the two nuclei.

15206+3342.—This is an evolved, single-nucleus galaxy in which the stellar and ionized gas components show a similar structure consisting of a central condensation and the inner, low surface brightness section of a tidal tail toward the northeast (better seen in the Hα light). The velocity dispersion outside the nuclear regions shows higher values than that in the nucleus. The major photometric and kinematic axes are orthogonal, and the largest velocity gradient is not found across the nucleus but along the region at 5 kpc northwest of the nucleus, where the inner section of the tidal tail connects with the main body of the galaxy. This tight correlation between the tail and the velocity pattern indicates that the observed velocities are associated with flows of gas along the tail (Arribas & Colina 2002).

15250+3609.—This is a single-nucleus galaxy with a compact Hα emission centered on the stellar nucleus with an additional faint Hα source at 7.7 kpc southeast of the nucleus. This source is identified with extranuclear tidal debris detected in *HST* optical images (Monreal 2004). The velocity field is such that the regions within 2 kpc of the nucleus present a small change in velocity while the external regions recede with velocities of about 100 km s^{-1} relative to the nucleus. The velocity dispersion also shows a complex structure with the highest measured values outside the nucleus and toward the south-southeast direction. It is likely that these kinematical features are associated with tidally induced motions in the outer regions of this ULIRG in which tidal tails and debris have been detected (Monreal 2004).

Arp 220.—This is the closest known ULIRG and a double-nucleus system with the two nuclei separated by 0.4 kpc. Because of internal extinction effects, the Hα emission and optical continuum peaks are located at about 0.5 and 0.75 kpc northwest of the near-IR, dust-enshrouded nucleus. The structure of the Hα distribution shows the clear effect of the central dust lane, dividing in two the ionized gas emission. The kinematics of the ionized gas on scales of less than 2 kpc around the nucleus is very complex. The Hα profile shows at least three different kinematic components, one that can be associated with rotation and two more interpreted as biconical outflows (Arribas et al. 2001). The velocity dispersion and velocity field shown in Figure 1 correspond to the much narrower [N II] λ6584 emission line.

IRAS 17208−0014.—This is a single-nucleus galaxy; however, the optical and near-IR continuum images show a different morphology owing to internal extinction effects, with the optical emission peak (i.e., optical nucleus) located at 1.3 kpc from the near-IR nucleus. A secondary emission peak in the optical, located at about 2.7 kpc southeast of the optical nucleus, is not associated with a second nucleus but with an extended, high surface brightness region in the host galaxy (Arribas & Colina 2003). The peak in the velocity dispersion coincides in position with the near-IR nucleus, while the velocity field is consistent with rotation around the nucleus (Arribas & Colina 2003).

3.2. *The Stellar and Warm Ionized Gas Structures*

The observed ionized gas and stellar light distributions are traced by the Hα emission and the optical and near-IR continuum, respectively. Differences in the optical and near-IR stellar light distribution are due to large differential extinction effects toward the nucleus in these galaxies. Of the eight ULIRGs in the sample, only two, the nearest ULIRG Arp 220 and IRAS 17208−0014, show the presence of a strong central dust lane obscuring the true nucleus in the optical. As a result, the optical nucleus, identified as the high surface brightness peak, is located at a distance of 0.75 kpc for Arp 220 (Arribas et al. 2001) and 1.3 kpc for IRAS 17208−0014 (Arribas & Colina 2003) from the near-IR nucleus. In other ULIRGs such as IRAS 08572+3915 and IRAS 12112+0305, the bright, dominant, near-IR

nucleus appears as a lower surface brightness region in the optical. Therefore, the internal extinction effects are those that would produce in some cases a wavelength dependence of the relative brightness of the nucleus with respect to the host galaxy while keeping, in general, the overall stellar light distribution, even in interacting pairs.

The observed gas and stellar distributions identified by the high surface brightness Hα and continuum light show decoupled structures with different morphologies in several ULIRGs. These differences are due to the presence of quiescent, extranuclear gas ionized by a central active galactic nucleus (AGN) pointing away from the tidal tails (Mrk 273; Colina et al. 1999), the presence of bright, tidally induced extranuclear star-forming regions along the tidal tails (IRAS 14348−1447) or far away (9 kpc or 6.″0) from the massive nucleus of the galaxy (IRAS 12112+0305; Colina et al. 2000), and the presence of circumnuclear gas ionized by a nuclear, dust-enshrouded starburst (Arp 220; Arribas et al. 2001).

In summary, although the sample of ULIRGs investigated with IFS is still small, offsets between the gas and stellar light distribution at the level of a few to several kpc seem to be fairly common (five out of eight) among ULIRGs, while substantial differences in their structure are less typical (three out of eight). On the other hand, the internal extinction effects are such that while keeping the overall stellar light distribution, they would produce in some ULIRGs a wavelength dependence change of the relative brightness of the stellar nucleus with respect to the host galaxy.

3.3. *Warm Ionized Gas Velocity Fields*

The velocity fields have been obtained measuring the centroid of the Hα emission line using the standard technique of simultaneous fitting of Gaussian components to the Hα and [N II] $\lambda\lambda$6548,6584 emission lines and assuming a single velocity component per line. For Arp 220 the measurement was done in a different way owing to the complexity of the Hα emission-line profile in the nuclear regions (Arribas et al. 2001). In this case, the velocity field is derived from the narrower [N II] λ6584 emission line.

The velocity fields of the ULIRGs investigated with IFS present a complex structure inconsistent, in general, with large, kiloparsec-scale ordered motions. Only one galaxy (IRAS 17208−0014) shows a velocity field consistent with that of a rotating disk of about 3 kpc in size (Arribas & Colina 2003), while one of the three velocity components identified in the central regions of Arp 220 (Arribas et al. 2001) could also trace a nuclear rotating disk already detected in molecular gas (Downes & Solomon 1998). In addition to IRAS 17208−0014 and Arp 220, there are other galaxies (e.g., IRAS 08572+3915) in which the major photometric and kinematic axes lie close in projection and could be considered candidates for rotating systems (Arribas et al. 2000). Higher angular resolution spectroscopy is needed to elucidate the presence of rotation in the inner regions ($\leq$1 kpc) of these galaxies. For the rest of the sample (seven galaxies in six ULIRGs), the largest velocity variations, characterized by peak-to-peak differences of 200–400 km s^{-1}, do not show a convincing case for rotation on scales of a few to several kpc. Evidence for inward flows (IRAS 15206+3342; Arribas & Colina 2002), outward motions associated with nuclear starbursts, and outer, tidally distorted regions of the galaxy (Arp 220; Arribas et al. 2001; Colina et al. 2004), motions along extranuclear star-forming regions and tidal tails (IRAS 12112+0305, IRAS 14348−1447; Monreal 2004), or flat velocity fields (Mrk 273, IRAS 15250+3609) are also present in these systems. The sample is still small, but there is so far no clear trend between the observed velocity field and the phase of the interaction/merging process traced by the stellar structure, i.e., intermediate phases identified with pairs (i.e., IRAS 12112+0305) and more advanced phases represented by double- (i.e., Arp 220), and single-nucleus (i.e., IRAS 17208−0014) galaxies.

In summary, the ionized gas velocity field in the central regions of ULIRGs on scales of a few to several kpc is dominated, in general, by merger-induced flows. Ordered rotational motions on these linear scales seem to be uncommon, even in the case of the more advanced mergers. In order to confirm these results, additional kinematic analysis of a larger sample is in progress.

3.4. *Warm Ionized Gas Velocity Dispersion Maps*

The velocity dispersion of the ionized gas was obtained at 0.425 times the FWHM of a Gaussian component fitted to the Hα emission line, after subtracting in quadrature the instrumental resolution and correcting for redshift. For Arp 220 the measurement was done in a different way because of the complexity of the Hα emission-line profile in the nuclear regions. In this case, the velocity dispersion is derived from the [N II] λ6584 emission-line profile assuming a single velocity component.

There are several important results worth mentioning. In the three ULIRGs identified as pairs of interacting galaxies (i.e., IRAS 08572+3915, IRAS 12112+0305, and IRAS 14348−1447), the velocity dispersion peak coincides with the dominant near-IR nucleus (IRAS 08572+3915 NW, IRAS 12112+0305 SW, and IRAS 14348−1447 SW). However, the velocity dispersion of the gas associated with the secondary nuclei is either undistinguishable (IRAS 08572+3915 SE) or even lower (IRAS 12112+0305 NE and IRAS 14348−1447 NE) than that of the surrounding, diffuse, extranuclear gas. Advanced interacting/merging systems, identified as double-nucleus (within 1.″0) and single-nucleus galaxies, do show different behaviors. There are ULIRGs such as IRAS 17208−0014 in which the peak of the velocity dispersion is offset with respect to the optical nucleus but coincides with the near-IR nucleus. However, other advanced mergers (Arp 220, IRAS 15206+3342, IRAS 15250+3609) do have the peak of the velocity dispersion offset from the near-IR nucleus by up to 2.″0–3.″0 (i.e., up to 3–5 kpc). Finally, there is one ULIRG (Mrk 273) located at about 3 kpc (i.e., 4.″0) from the nucleus in which the velocity dispersion in the nuclear region is not distinguishable from that of the gas ionized by the central AGN.

In summary, the nucleus (of the brightest galaxy in binary systems) usually has the highest velocity dispersion and therefore seems to trace the mass. However, the high-velocity dispersions of the extranuclear gas, typically between 70 and 200 km s^{-1}, are associated with tidally induced flows and do not trace mass concentrations, in general, in these systems.

3.5. *Gaseous and Stellar Central Velocity Amplitude*

To be consistent with previous near-IR stellar measurements, the central velocity amplitude for the ionized gas is defined as half the peak-to-peak velocity difference at radii of 1.″0–2.″0 on either side of the galaxy. A comparison with respect to similar measurements for the stellar and cold gas component, traced by the near-IR CO absorption bands and CO millimeter emission line, respectively, is presented in Figure 2 (see also Table 3 for the specific values). The stellar and ionized gas velocities do agree in general ($V_{\rm gas}^{\rm warm}/V_{\rm stellar} = 0.92 \pm 0.37$; see Table 3 for specific values), although discrepancies exist, most notably for the southwestern nucleus of galaxy IRAS 14348−1447, where

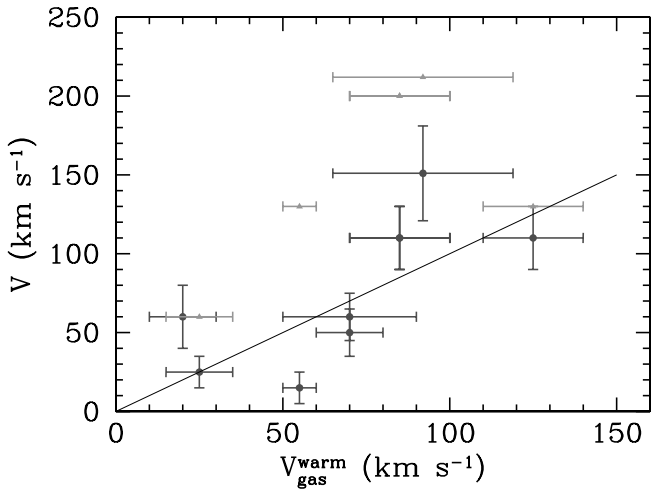

FIG. 2.—Central stellar (*filled circles*) and cold molecular gas (*filled triangles*) velocity amplitudes vs. the warm ionized gas values obtained from our IFS. Uncertainties are only given for the stellar and ionized gas measurements, since no published values for the cold molecular gas are available. The line represents a slope of 1. [*See the electronic edition of the Journal for a color version of this figure.*]

the low-velocity amplitude of the stellar component is 3 times that of the ionized gas. On the other hand, the cold molecular gas shows a central velocity amplitude a factor of 2 larger than that of the stars and ionized gas (average ratio of 1.9 ± 0.6 combining the nine pairs of measurements for which either stellar and cold gas, or warm and cold gas exist). These results suggest that while the stars and ionized gas generally share the same velocity field in the central regions, the cold molecular gas could have a different velocity field. Stellar and gaseous kinematic data for a larger sample of ULIRGs need to be obtained to investigate this further.

There are galaxies for which serious discrepancies among the derived velocities are found. The molecular gas velocity amplitude in Mrk 231, Mrk 273, and IRAS 23365+3604 appears to be a factor of at least 2 larger than that of the ionized gas or stellar component. The reason(s) for the discrepancies in these galaxies is not clear. Two (Mrk 231 and Mrk 273) of the three galaxies have a nuclear rotating disk of cold molecular gas (Downes & Solomon 1998). It could well be that the spatial distribution and kinematics of the stars and ionized gas do not share the rotating disk structure of the cold gas. On the other hand, Mrk 231 and Mrk 273 have a nucleus classified as Seyfert. In these cases the AGN itself could be affecting the kinematics, at least, of the ionized gas. An indication that this could be happening in Mrk 273 is the fact that the velocity dispersion traced by the Hβ and [O III] λ5007 lines are significantly different, with the [O III] line a factor of 1.4 broader than the Hβ line (see Table 3). Arp 220 is another galaxy that shows a discrepancy between the different measurements (see Table 3 and Fig. 2). The central velocity ranges from about 92 km s^{-1} for the ionized gas to 212 km s^{-1} for the molecular gas (Downes & Solomon 1998), with a value of 151 km s^{-1} for the stellar component (Tacconi et al. 2002). The central velocity field of Arp 220 is by far the most complex of all ULIRGs studied with IFS. The complexity of the velocity field and line profile is not a consequence of Arp 220 being the closest ULIRG, i.e., resulting in a higher linear scale resolution for the same angular resolution. Arp 220 also shows a CO emission-line profile that is intrinsically broader than that in most ULIRGs (Solomon et al. 1997; J. Gracia et al. 2005, in preparation). In fact, if studied in detail, the discrepancies in Arp 220 are removed (ionized and molecular gas components) or highly reduced (stellar vs. gas).

TABLE 3
ULIRG SAMPLE: STELLAR AND GAS KINEMATICS

IRAS Galaxy	$\sigma_{stellar}$ (km s^{-1})	$V_{stellar}$ (km s^{-1})	Reference[a]	σ_{gas}^{cold} (km s^{-1})	V_{gas}^{cold} (km s^{-1})	Reference[a]	σ_{gas}^{warm} (km s^{-1})	V_{gas}^{warm} (km s^{-1})	Reference[b]
08572+3915 NW	...	...	...	106	...	E02	113 (14)	46 (7)	ACB00
08572+3915 SE	...	...	...	...	...	...	47 (10)	91 (12)	ACB00
Mrk 231	120 (10)	25 (10)	T02	81	60	DS98	...	25 (10)	T02
Mrk 273[c]	285 (30)	110 (20)	T02	160	200	DS98	243 (29)	85 (15)	[O III]
	160 (60)	...	J99				174 (38)		Hβ
12112+0305 NE	...	...	...	170	...	E02	130 (21)	150 (20)	This work
12112+0305 SW	...	...	...	127	...	E02	160 (12)	70 (20)	This work
14348-1447 NE	150 (25)	50 (15)	G01	149	...	E02	147 (12)	70 (10)	This work
14348-1447 SW	170 (14)	60 (20)	G01	127	...	E02	196 (16)	20 (10)	This work
15206+3342	...	...	...	85	...	SA88	90 (10)	45 (10)	AC02
15250+3609	150 (10)	60 (15)	T02	...	...	...	168 (15)	70 (20)	
Arp 220[d]	166 (10)	151 (30)	T02	149	212	DS98	185 (10)	92 (27)	This work
							115 (30)	225	ACC01
17208-0014	229 (15)	110 (20)	G01	159	130	DS98	200 (20)	125 (15)	AC03
20087-0308	219 (14)	50 (15)	G01	170	...	SDRB97	...	...	...
23365+3604	145 (15)	<15 (10)	G01	85	130	DS98	...	55 (5)	G01

[a] Velocities not corrected for inclination or spatial resolution effects.

[b] The reference indicates the original publication although new measurements have been done to obtain homogeneous data. The velocities indicate half the velocity differences observed on either side of the nucleus, at radii of 1.″5–2.″0, not corrected for inclination or spatial resolution effects. The values presented for Mrk 231 and IRAS 23365+3604 come from near-IR emission-line measurements by Tacconi et al. (2002) and Genzel et al. (2001), since no optical emission-line measurements are available.

[c] The velocity dispersion measurements for the warm gas are taken from IFS data using independent measurements of the Hβ and [O III] lines.

[d] The velocity dispersion and velocity amplitude measurements used in this paper are obtained from a single component fit to the [N II] λ6584 line. The second set of values (presented here for reference) correspond to the rotational velocity field derived from the two-dimensional, three-velocity component fit of the Hα line profile (ACC01).

REFERENCES.—(ACB00) Arribas et al. 2000; (ACC1) Arribas et al. 2001; (AC02) Arribas & Colina 2002; (AC03) Arribas & Colina 2003; (DS98) Downes & Solomon 1998; (E02) Evans et al. 2002; (G01) Genzel et al. 2001; (J99) James et al. 1999; (SA88) Sanders et al. 1988; (SDRB97) Solomon et al. 1997; (T02) Tacconi et al. 2002.

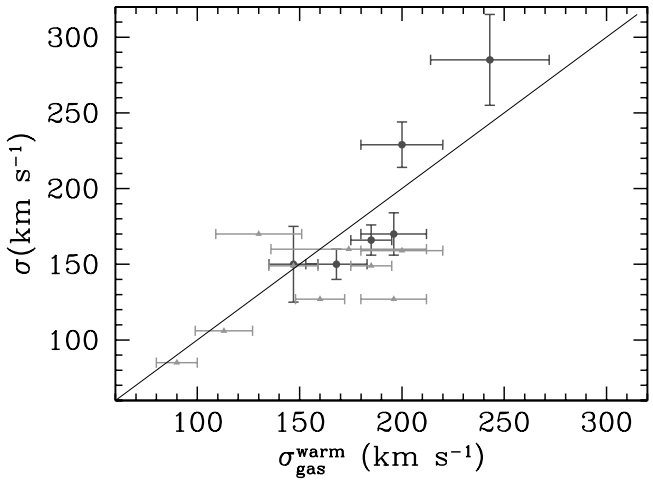

FIG. 3*a*

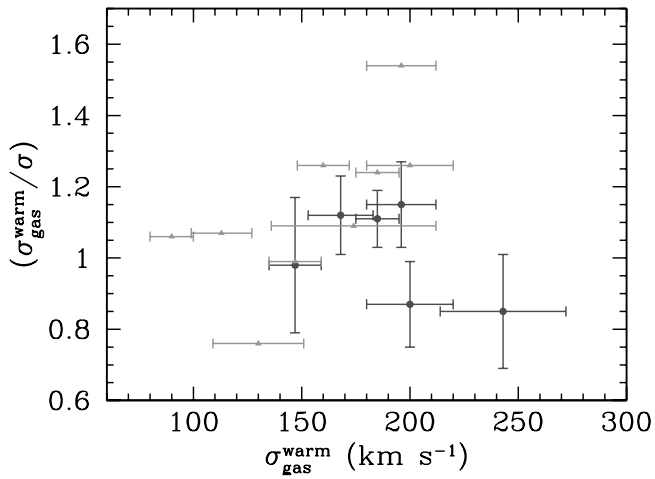

FIG. 3*b*

FIG. 3.—(*a*) Central stellar (*filled circles*) and cold molecular gas (*filled triangles*) velocity dispersion vs. the warm ionized gas values obtained from our IFS. Uncertainties are only given for the stellar and ionized gas measurements since no published values for the cold molecular gas are available. The line represents a slope of 1. (*b*) Ratios of the stellar and cold molecular gas velocity dispersions to the warm, ionized gas values. [*See the electronic edition of the Journal for a color version of this figure.*]

Our detailed two-dimensional, multiple component analysis (Arribas et al. 2001) identifies the presence of nuclear rotating gas with a velocity amplitude of 225 km s^{-1} and minor kinematic axis of 135° ± 15°, in good agreement with the values derived for the disk of molecular gas, 212 km s^{-1} and 130° (Downes & Solomon 1998). On the other hand, although the amplitude of the central stellar velocity is sightly lower (151 km s^{-1}), the velocity amplitude through the eastern nucleus and along the position angle (P.A.) 52, i.e., about 10° away from the major kinematic axis, corresponds to 185 ± 30 km s^{-1} (Genzel et al. 2001) and is therefore in better agreement with the values corresponding to the gaseous components.

Aside from the possibility of the stellar, cold, and warm gaseous components having different intrinsic kinematics, there are several effects that could explain the discrepancies among the observed velocities, with more than one effect most likely involved in each galaxy. The near-IR stellar measurements are based on narrow-slit (0.″6 width) spectroscopy centered on the nucleus and oriented along a given P.A. As shown in Figure 1, the velocity fields in ULIRGs do not in general show a regular rotation pattern, and therefore the amplitude of the velocity difference measured using long-slit spectroscopy would depend on the selected position angle and the accuracy of the positioning of the narrow slit on the nucleus. On the other hand, optical measurements could be affected in some cases by the differential internal extinction that usually increases toward the nucleus. Finally, differences in the angular resolution would also have some impact, since any reduction in the spatial resolution would tend to reduce the true amplitude of the velocity field. Despite all these technical and observational effects, it is important to emphasize that the three independent measurements (stellar, warm, and cold gas) taken along the major axis of the velocity field agree within their uncertainties for the only ULIRG (IRAS 17208−0014) for which our velocity field, based on IFS, is consistent with that of an inclined rotating disk (Arribas & Colina 2003). This is also true for Arp 220, where, as explained above, our detailed multiple component analysis (Arribas et al. 2001) identifies the presence of nuclear rotating gas with kinematical properties similar to those of the previously detected disk of cold molecular gas (Downes & Solomon 1998).

In summary, discrepancies among the different velocity tracers are a natural consequence of the disordered velocity field present in these galaxies and of the use of different observational techniques. Agreement appears to exist between the observed velocities of the stellar and gaseous components in the two galaxies for which the central velocity field is consistent with rotation. Even taken into account the discrepant values, the ratio of the central ionized gas to stellar velocity amplitude is, on average, close to unity (0.92 ± 0.37), indicating the warm gas and the stars are most likely sharing the same velocity field. The scatter on the observed velocity ratio can most likely be reduced by using more homogeneous observational techniques (optical and near-IR IFS, similar angular resolution, etc.). The central velocities of the cold gas are systematically larger (by almost a factor of 2) than those of the stars and warm gas. Studies with a larger sample of galaxies are needed to confirm this result and to favor the existence of a different velocity field for the cold gas component (i.e., rapidly rotating nuclear disk versus pressure supported stellar bulge; see also § 3.6).

3.6. *Gaseous and Stellar Central Velocity Dispersion*

A comparison of the central ionized gas velocity dispersion with respect to similar measurements for the stellar and cold gas components is presented in Figure 3 (see also Table 3 for the specific values). The velocity dispersion was derived from the profile (FWHM) of the Hα emission line corresponding to the fiber associated with the near-IR continuum emission peak, after correcting for instrumental and redshift effects. For Mrk 273, two independent measurements were obtained for the Hβ and [O III] λ5007 lines as they have different profiles. It is interesting to mention that the velocity dispersion derived from the [O III] line agrees with the stellar velocity dispersion obtained from near-IR absorption lines, while the Hβ-derived dispersion is similar to the molecular gas velocity dispersion (see Table 3 for specific values). This result is not well understood and requires further investigation with additional high spatial resolution data.

The stellar and cold gas velocity dispersions correlate well with the values obtained for the warm ionized gas (see Fig. 3*a*) and are for the most part in agreement within the uncertainties (see Fig. 3*b*). There is a tight correlation between the warm

ionized gas and stellar velocity dispersions with an average of 1 and a low scatter ($\sigma_{\rm gas}^{\rm warm}/\sigma_{\rm stellar} = 1.01 \pm 0.13$) This result supports the idea that the ionized gas central velocity dispersion is dominated by the gravitational potential of the system (i.e., its mass) as traced by the stellar velocity dispersion. Additional gas motions like starbursts or AGN induced outflows, identified in some galaxies by the presence of additional secondary velocity components in the optical emission lines, do not play a significant role, in general. On the other hand, as for the central velocity (see § 3.5), the deviations of the cold molecular gas with respect to both the stellar and ionized gas velocity dispersions are larger, i.e., $\sigma_{\rm stellar}/\sigma_{\rm gas}^{\rm cold} = 1.33 \pm 0.25$ and $\sigma_{\rm gas}^{\rm warm}/\sigma_{\rm gas}^{\rm cold} = 1.14 \pm 0.22$, respectively. This result suggests again that the kinematics of the cold molecular gas in the central regions of these galaxies is, in general, not the same as that of the stars and warm gas. In fact, the central velocity-to-velocity dispersion (V/σ) ratio for the cold gas (1.15 ± 0.36; five values) suggest that the molecular gas is more rotationally supported than the stars (0.42 ± 0.23; eight values) and ionized gas (0.63 ± 0.50; 11 values).

Although the number of galaxies is small and the velocity dispersion measurements have not been obtained with the same angular resolutions, the good agreement between the stellar and warm ionized gas values indicates that a robust measurement of the central velocity dispersion can be obtained through the analysis of either absorption or emission lines at different wavelengths, i.e., independent of the method used, provided that similar angular resolutions are available. This result supports and extends to ULIRGs similar conclusions derived for a local sample of late-type galaxies (Kobulnicky & Gebhardt 2000), where the ionized gas and stellar velocity dispersions give comparable results, within the uncertainties. Thus, even if starburst or AGN-related outflows exist in these galaxies, their kinematical effect does not affect the derivation of the central velocity dispersion based on measurements of the width (FWHM) of the optical emission lines. On the other hand, there are indications suggesting that the cold molecular gas does not share the same velocity field as the stars and ionized gas and could be more rotationally supported. Since the studied sample is small, further investigations with a larger sample are required before deriving any firm conclusion on this.

4. DISCUSSION

4.1. *Mass Derivations in Low-z ULIRGs: Stellar and Gaseous Kinematic Tracers*

We have shown (see § 3.3) that the velocity field of ULIRGs, even for those showing the morphological characteristics of being in advanced phases of the merging process generally do not follow the pattern of a rotating system, at least not on scales of a few to several kpc. In the present sample, only one (IRAS 17208−0014) of the 11 galaxies (in eight ULIRGs) with IFS has been identified as a rotating system, while in another galaxy (Arp 220), the presence of the already known rotating disk (Solomon et al. 1997) has been inferred after detailed velocity decomposition of the emission-line profiles (Arribas et al. 2001). In general, the largest velocity amplitudes are detected outside the nuclear regions and lack alignment with the photometric major axis. Therefore, the disordered structure of the velocity field of ULIRGs indicate that the peak-to-peak velocity amplitudes do not trace rotation and preclude their generalized use as tracers of the dynamical mass of these systems within a radius of a few to several kpc. Even in galaxies like IRAS 17208−0014, where a rotating system has been identified, the uncertainty in the mass estimate can be large as a result of the uncertainty on the determination of the inclination, in particular if the system is close to face-on.

On the other hand, the good agreement between the central velocity dispersion measurements obtained from the different tracers, in particular the stellar and warm ionized gas, is especially encouraging. The velocity dispersion can be used to obtain the dynamical mass of these galaxies, if the central regions are assumed virialized, and if the stellar mass distribution is known (see discussion in § 4.2). Assuming virialization, the dynamical mass of a system is given as

$$M_{\rm dyn} = m10^6 R_{\rm hm}\sigma^2\ M_\odot \quad (1)$$

or

$$M_{\rm dyn} = 0.71m10^{-5} R_{\rm hm}\sigma^2 m_* \quad (2)$$

where $R_{\rm hm}$ is the half-mass radius in kiloparsecs and σ is the central velocity dispersion in kilometers per second. The factor m is a function of the assumed mass distribution and ranges from 1.4 for a King stellar mass distribution with a ratio of tidal to a core radius of 50 that adequately represents ellipticals (Bender et al. 1992; Tacconi et al. 2002) to 1.75 for a polytropic sphere with a density index covering a range of values (Spitzer 1987) and 2.1 for a de Vaucouleurs mass distribution (Combes et al. 1995).

The half-mass radius is not an observable and cannot be measured directly. It has to be inferred indirectly by measuring the half-light radius (R_e) through high spatial resolution near-IR imaging (e.g., *H*-band *HST* imaging) and assuming that the near-IR continuum light distribution traces the mass (see § 4.2 for a discussion on the reliability of this assumption). Considering the mass scaling factor for a polytropic sphere (i.e., an m-value of 1.75) and that an m_* galaxy has a mass of $1.4 \times 10^{11}\ M_\odot$ for a Salpeter initial mass function (Cole et al. 2001), masses for the ULIRG subsample (eight ULIRGs, 11 galaxies) with IFS, including for the first time independent mass estimates for each of the galaxies in the pairs IRAS 08572+3915, IRAS 12112−0305, and IRAS 14348−1447, have been obtained from the observed central ionized gas velocity dispersion. The estimated masses cover the $0.03m_*$–$1.1m_*$ mass range, with an average value of $0.4m_* \pm 0.3m_*$. With the exception of Mrk 273, the derived masses agree remarkably well, to within $0.1m_*$, with the corresponding values derived from near-IR stellar absorption lines and ground-based *K*-band images (see Table 4 for specific values). Therefore, the dynamical mass estimates based on the ionized gas central velocity dispersion confirm and extend to pairs the conclusion already reached for single-nucleus systems (Tacconi et al. 2002) that ULIRGs are moderate-mass systems (i.e., $m \leq m_*$). Although this is still a small sample, the agreement between the gaseous and stellar mass estimates is very encouraging and supports the idea that consistent mass estimates can be obtained independent of the method and physical tracer used. Additional multifrequency measurements have to be obtained in order to corroborate the results with a larger sample.

Mrk 273 shows a peculiar behavior that deserves further investigation with additional data. Of the five ULIRGs (six galaxies) with available gaseous and stellar measurements, Mrk 273 is the only galaxy with a Seyfert nucleus. The velocity dispersion derived from the [O III] line is much higher than that of the Hβ line. There is evidence that the [O III]–emitting gas has

TABLE 4
ULIRG Sample. Dynamical Mass Estimates

IRAS Galaxy	R_e^{K}[a] (kpc)	R_e^{K}, R_e^{Hb} (kpc)	R_e^{Hc} (kpc)	M_{dyn}^{gasd} (m_*)	$M_{dyn}^{stellare}$ (m_*)
08572+3915 NW	...	0.15, 0.74	0.91	0.1	...
08572+3915 SE	...	...	1.00	0.03	...
Mrk 231	0.3	...	0.20	...	...
Mrk 273	2.0	0.96, 1.25	1.47	0.6–1.1	2.0
12112+0305 NE.....	...	...	1.89	0.4	...
12112+0305 SW.....	...	0.48, 0.85	0.75	0.3	...
14348-1447 NE.....	3.0	...	1.70	0.5	1.0
14348-1447 SW.....		0.72, 1.15	1.3	0.6	
15206+3342	...	...	2.47	0.3	...
15250+3609	1.2	0.70, 1.08	1.1	0.4	0.3
Arp 220	0.55	0.62, 1.17	0.79	0.3	0.2
17208-0014	1.4	0.94, 1.18	1.40	0.7	0.9
20087-0308	3.3	...	1.64	...	2.0
23365+3604	4.8	...	5.47	...	1.25

[a] *K*-band effective radii as given in Tacconi et al. (2002). Value for IRAS 14348−1447 represents the effective radii of the entire double-nucleus system as explained in Genzel et al. (2001).

[b] *K* (first value) and *H*-band half-light radii within a 3 kpc diameter aperture as given in Scoville et al. (2000) and corrected for the different H_0 (75 km s^{-1} Mpc^{-1}) used in Scoville et al. Not clear how the effective radius has been measured for the double-nucleus systems (i.e., IRAS 12112−0305 and IRAS 14348−1447), but presumably the values correspond to the dominant nucleus.

[c] *H*-band effective radii measured from the F160W NICMOS/*HST* archival images, except for IRAS 15206+3342 and IRAS 23365+3604, for which no near-IR *HST* imaging was available and F814W WFPC2/*HST* images were used instead. The uncertainties are about 0.1 kpc or less for single-nucleus ULIRGs and 0.2–0.3 kpc for pairs.

[d] Dynamical mass derived from expression (2) of § 4.1 using the nuclear velocity dispersions derived from our INTEGRAL data (Table 3), the effective radii given in the fourth column, and assuming $m_* = 1.4\times10^{11}$ $M_\odot$. The two values for Mrk 273 are derived for the two independent velocity dispersion measurements obtained from the Hβ and [O III] lines.

[e] Dynamical mass derived from expression (2) with an *m*-value of 1.75, using the near-IR stellar velocity dispersion, and effective radii given in Tacconi et al. (2002). The mass value for IRAS 14348−1447 corresponds to the entire system and is compared with the sum of galaxies IRAS 14348−1447 NE and IRAS 14348−1447 SW in the third column. The mass value for Mrk 231 is not included because the light profile is dominated by the Seyfert 1 nucleus.

a secondary, high-velocity component in the circumnuclear regions (Colina et al. 1999). However, while the [O III]–derived velocity dispersion agrees with the most recent stellar-derived measurements (Tacconi et al. 2002), the Hβ-derived value agrees with previous stellar (James et al. 1999) and molecular gas (Downs & Solomon 1998) derived values (see Table 3 for details).

4.2. *Reliability of Mass Estimates in Low-z ULIRGs*

The accuracy of the mass estimates of ULIRGs relies on the one hand on the reliability of the central velocity dispersion measurements and the knowledge of the mass distribution of the host galaxies, and on the other hand on the validity of the virialization assumption for these interacting/merging systems. In the following, we discuss the uncertainties and caveats that have to be taken into account when estimating the mass of ULIRGs. As shown previously (see § 3.6), the derivation of the central velocity dispersions based on stellar and ionized gas atomic lines give consistent results in general.

The mass distribution cannot be derived directly from the observations and has to be inferred from the stellar light distribution, assuming light traces mass in these systems. This process has a number of uncertainties associated with it, mainly due to internal extinction effects and light contributions from an AGN or nuclear starbursts. Because of the large amount of gas and dust and their complex geometry, ULIRGs are systems characterized by having an irregular structure of patchy dust lanes producing large internal extinctions toward the nucleus and large extinction gradients (i.e., two-dimensional differential effects). As extinction in the near-IR is a factor of 5–10 smaller than that in the optical, a proper way to minimize these effects is to measure the half-light radius in the *H* or *K* bands, as done in this work. However, as the internal extinction in ULIRGs generally decreases outward, the half-light radius derived directly from near-IR imaging would be larger than the true value, if a two-dimensional, extinction correction is not applied, as is often the case. Detailed two-dimensional *H*-band internal extinction corrections in a few ULIRGs indicate that the uncertainty in the uncorrected half-light radius is less than 15% (Monreal 2004). On the other hand, near-IR continuum light traces not only the old stellar population but also the light from an AGN or massive starbursts. The mass-to-light ratio of AGNs and young starbursts is several orders of magnitude smaller than that of intermediate-to-old (several Myr to few Gyr) stellar populations; therefore, even a small mass contribution in the form of a nuclear starburst and/or accreting black hole would increase the near-IR flux in the central regions. Thus, the measured half-light radius would be smaller than the true value by an unknown factor that would depend on the exact contributions of AGNs and young stellar populations to the observed light distribution in a given galaxy. In the few ULIRGs with a luminous, compact AGN such as Mrk 231, this has to be taken into account before establishing the half-light radius of the host galaxy. For the more general situation in which a nuclear starburst is present, if 1% of the total stellar mass is in the form of young (i.e., less than 10 Myr old) stars, their contribution to the *H*-band luminosity would be about 10% of the total, if age-dependent mass-to-light ratios are considered (Starburst99; Leitherer et al. 1999). The measurements of the effective radius for the sample of galaxies by different groups using different set of data or different criteria are presented in Table 4. Based on this comparison and the considerations above regarding the differential extinction and nuclear starbursts, the uncertainty of the value of the effective radius can be established as 20%.

The other relevant aspect when deriving masses of ULIRGs is the validity of the assumption of virialization in these interacting/merging systems, and that the mass distribution is close to that of ellipticals. To first order these assumptions seem to be reasonable. Assuming light traces mass, since the half-light near-IR radius of ULIRGs is only a few kpc (Scoville et al. 2000; Colina et al. 2001; Tacconi et al. 2002), the crossing time of most stars in these systems is rather short ($\sim$10 Myr) when compared with the dynamical time ($\sim$100 Myr) of the interaction and merging process in which violent relaxation tends to produce a de Vaucouleurs light profile over a large range in radius ($\leq$10 kpc; Mihos & Hernquist 1996). This is consistent with the results of surveys concluding that 37% of the double-nucleus ULIRGs show either a pure elliptical-like or an elliptical/disk-like light profile, while this fraction increases up to 73% of the single-nucleus ULIRGs (Veilleux et al. 2002).

Therefore, considering uncertainties in the assumed mass distribution represented by the mass factor $m = 1.75 \pm 0.35$ in expressions (1) and (2) of 20% in the effective radius and 15% in the central velocity dispersion (see § 3.6), respectively, the dynamical mass in ULIRGs can be estimated with an uncertainty of 40%–50%, provided virialization applies.

4.3. *Implications for Mass Estimates in High-z Star-forming Galaxies*

Establishing the mass assembly in galaxies as a function of redshift is one of the main goals of modern observational cosmology that would help to constrain the galaxy formation scenarios (Illingworth & Bouwens 2005). Stellar mass estimates for high-z galaxies can and will be obtained through detailed stellar energy distribution modeling of deep multiband photometry covering a wide range in wavelength (Barmby et al. 2004; Bell et al. 2003, Papovich et al. 2001; Shapley et al. 2001, 2004). This will also be the approach to follow with future instruments such as NIRCAM and MIRI cameras on board the *JWST*, covering the wavelength range from about 0.6 to 27 μm, i.e., the entire ultraviolet to near-IR rest frame for high-redshift galaxies.

The gas content most likely represents a large fraction of the mass in high-z galaxies; therefore, stellar mass measurements not only have their own uncertainties (internal extinction effects, universality of the initial mass function slope and lower mass limit, etc.; see also Dickinson et al. 2003) but intrinsically represent a lower limit to the dynamical mass in these systems. More realistic estimates of the dynamical mass in high-z sources have to be derived exclusively through kinematic tracers such as the central velocity amplitude or velocity dispersion using either absorption or emission-line measurements, as in low-z ULIRGs. Since good signal-to-noise ratio measurements of stellar absorption lines are, in general, more difficult than those of emission lines, the dynamical mass estimates are likely to be restricted, in practical terms, to the use of molecular emission lines in the millimeter wavelength range (Genzel et al. 2003; Neri et al. 2003) and optical (near-IR) atomic emission lines shifted into the near-IR (mid-IR) wavelength range for high-z galaxies (Pettini et al. 2001; Erb et al. 2003, 2004; Tecza et al. 2004). In addition, typical subarcsecond (0.″2) near-IR observations of high-z galaxies will correspond to a linear scale of about 1.5 kpc, similar to the average scale in our low-z sample of ULIRGs for which IFS is available (see § 2 and Table 2).

Discrepancies between the stellar and dynamical mass estimates have already been obtained in a small sample of UV-selected, high-z galaxies (Shapley et al. 2004). The stellar mass, derived from multiwavelength photometry modeling, is up to 10 times higher than the dynamical mass obtained from long-slit Hα velocity dispersion measurements. This result underlines, as already mentioned by these authors, the importance of understanding the origin of the discrepancies before establishing any firm conclusion about the assembly of mass in galaxies as a function of redshift. In the following we present the similarities between our sample of low-z ULIRGs and high-z star-forming galaxies such as LBGs and SMGs, and we discuss some caveats that should be taken into account when deriving mass in high-z objects using emission-line kinematic tracers.

4.3.1. *ULIRGs and High-z Star-forming Galaxies: Mergers at Low and High Redshift*

Star-forming galaxies with high star formation rate (>10 $M_{\odot}$ yr^{-1}) have been identified in large numbers at high redshifts as strong ultraviolet emitters (LBGs; Steidel et al. 2004 and references therein) and strong far-IR sources (SMGs; Blain et al. 2002 and references therein). As for the low-z sample of ULIRGs presented in this study, a large fraction of high-z (>2) star-forming galaxies present the morphological features characteristic of interacting/merging systems in different phases of their evolution. There is a predominance of irregular and complex morphologies in luminous SMGs, suggesting that major mergers are common for these galaxies (Chapman et al. 2003b). On the other hand, LBGs and UV-selected, high-z star-forming galaxies do often show irregular and distorted morphologies (Giavalisco et al. 1996; Erb et al. 2003, 2004), suggesting that interaction/merging is also involved in these galaxies. A recent quantitative analysis of the morphology of galaxies detected in the WFPC2 and NICMOS Hubble Deep Field North concludes that the fraction of galaxies consistent with undergoing a major merger increases with redshift for all galaxies, with the highest fraction (40%–50%) of objects identified as LBGs (Conselice et al. 2003). Moreover, at redshifts above 2, more than 80% of the stellar mass is in objects with peculiar morphology, and the quantitative structural analysis of these objects indicates that they are involved in major mergers (Concelise et al. 2005). In addition, the optical colors, luminosities, sizes, and star formation rates derived for SMGs (Blain et al. 2002; Frayer et al. 2004) indicate that these galaxies are the high-z analogs of the low-z (U)LIRGs (Arribas et al. 2004).

Differential extinction plays a significant role in the observed relative surface brightness of the different regions in our low-z ULIRGs. In particular, the high surface brightness optical continuum peak (i.e., optical nucleus) does not necessarily coincide with the true (near-IR) nucleus (Arp 220, IRAS 17208−0014; see § 3.2). The same is also true for the distribution of the ionized gas in several ULIRGs, in which the Hα high surface brightness peak is displaced by up to several kpc with respect to the near-IR (or optical) peak as a result of differential extinction (0.75 kpc, Arp 220), the presence of bright, tidally induced, extranuclear star-forming regions (9.3 kpc, IRAS 16007+3743; García-Marín et al. 2005), or both (7.5 kpc, IRAS 12112+0305). These effects produce different morphologies in the ionized gas and stellar light distributions, as detected in many of our ULIRGs (see Fig. 1). Changes in the morphology of the stellar and ionized gas, as well as spatial separations of several kpc between their respective continuum and emission-line high surface brightness peaks, have also been detected in one SMG and a number of LBGs thus far. Recent near-IR IFS of the SMG SMM J14011+0252 at a redshift of 2.565 identifies the strongest Hα emission peak 1.″5 (i.e., 12 kpc at the redshift of this source) away from the optical (rest-frame) continuum peak (Tecza et al. 2004). The LBG Q0256−000 C17 at a redshift of 3.28 shows two [O III]–emitting regions separated by 24 kpc, with one of the regions being associated with a very faint continuum source (Pettini et al. 2001). Similarly, in the LBG Q0347−C5 at a redshift of 3.23, the [O III] emission is not spatially coincident with the UV continuum peak (Pettini et al. 2001).

4.3.2. *Dynamical Mass Estimates from Velocity Amplitudes*

The results presented in § 3 based on integral field optical spectroscopy have shown that, in general, the amplitude of the ionized gas velocity field in low-z ULIRGs is not a reliable dynamical mass indicator because (1) the projected orientation of the photometric and kinematic major axis do not coincide, (2) the velocity field does not show a rotational pattern on scales of a few to several kpc, and (3) the velocity gradients, in some cases with peak-to-peak velocity amplitudes similar to those expected in massive rotating systems, are associated with the relative velocities of the merging galaxies, flows in tidal tails, or in extranuclear, high surface brightness, star-forming regions.

If, in general, high-z star-forming galaxies such as LBGs and SMGs are merging systems like low-z ULIRGs, their large-scale (few to several kpc) velocity field will also be dominated by the tidal flows induced by the merging process. Tidal motions due to mergers have already been suggested in a sample of

high-z, UV-selected elongated galaxies (Erb et al. 2003, 2004), where there was a lack of evidence for rotation (i.e., no detection of tilted Hα emission line), in spite of the fact that the slit was nearly aligned with the major photometric axes in most of the galaxies (11 of 13). Moreover, tilted Hα lines are equally detected in these galaxies when the long slit is positioned away from the major photometric axes (Erb et al. 2003, 2004), as expected if their kinematics is similar to that of our low-z ULIRG mergers. Therefore, mass derivations in high-z star-forming galaxies based on long-slit spatially resolved Hα velocity amplitudes positioned along the rest-frame ultraviolet-optical photometric major axis (Erb et al. 2003, 2004) should be treated with caution and not considered a reliable dynamical mass tracer in general (see § 4.2).

On the other hand, dynamical mass estimates of high-z star-forming galaxies can and will be derived, at least in SMGs, from the cold molecular gas velocity field using radio interferometers (IRAM, ALMA). Millimeter wave observations of the galaxy SMM J02399−0136 with the Plateau de Bure interferometer at a redshift of 2.8 have identified it as a very massive galaxy assuming that the cold molecular gas, traced by the CO (3–2) line, is distributed in a rotating disk (Genzel et al. 2003). Although the double-horn CO line profile presents a compelling case for rotation in this galaxy, the use of the cold molecular gas velocity amplitude to establish the mass in SMGs should be treated in general with caution. Since SMGs appear to be high-z (U)LIRGs, an understanding of the discrepancy observed in our low-z ULIRG sample between the molecular gas and the stars and ionized gas central velocity amplitudes (average ratio of 1.9 ± 0.6; see § 3.6) is required before using the cold gas velocity as a dynamical mass tracer.

4.3.3. *Dynamical Mass Estimates from Central Velocity Dispersions*

Most dynamical mass estimates of high-z star-forming galaxies are being derived from velocity dispersion measurements using the velocity profiles of optical emission lines such as [O III] λ5007 (Pettini et al. 2001) and Hα (Erb et al. 2003, 2004). The central stellar and ionized gas velocity dispersion measurements in low-z ULIRGs give homogenous results and can be considered equally good tracers of the dynamical mass of these galaxies (see § 3.6). However, some caveats have to be kept in mind, in particular when integrated spectra or long-slit spectroscopic techniques are used. Our IFS of ULIRGs has shown (see § 3.4) that often the region with the largest velocity dispersion does not coincide with the nucleus of the galaxies, at least not with the secondary nucleus, but rather is associated with large-scale, tidally induced motions. In addition, the observed optical and near-IR continuum light peaks are spatially displaced in some galaxies (see § 3.2). Moreover, similar to that found in some SMGs (Tecza et al. 2004) and LBGs (Pettini et al. 2001), the ionized gas distribution in ULIRGs is often decoupled from the stellar distribution, with the high surface brightness emission line and continuum peaks spatially separated by several kpc as a result of differential extinction, the presence of luminous extranuclear star-forming regions, or both (see § 3.2). Therefore, to use the ionized gas velocity dispersion value as a reliable mass tracer for high-z galaxies, a prior knowledge of the stellar light distribution traced by high angular resolution optical or preferentially near-IR, rest-frame continuum imaging is required in order to properly identify the nucleus of the galaxy, or nuclei in pairs or multiple systems. This is particularly important to keep in mind if velocity dispersions are derived from long-slit spectroscopy measurements in order to properly center and orient the narrow slits.

Millimeter CO emission lines are also being used to obtain the dynamical mass of SMGs (Neri et al. 2003). The median CO line width (420 km s^{-1}) derived for a sample of five high-z ($\sim$2.7) SMGs have been used to conclude that the dynamical masses of SMGs are typically a factor of 6 larger than LBGs at similar redshift (Tecza et al. 2004). This conclusion is potentially important but has to be treated with caution, since different tracers have been used to derive the dynamical mass in SMGs (CO molecular line) and LBGs (optical emission lines). There are indications in our low-z ULIRG sample that the cold molecular gas could not be sharing the same kinematics as the stars and ionized gas and could be more rotationally supported (see § 3.6). If this were also the case in high-z LBGs and SMGs, a direct comparison of the dynamical masses of different samples of galaxies based on cold and warm gas velocity dispersion values would not be valid without applying a correction to take into account the different kinematics of the gaseous components.

5. CONCLUSIONS

The velocity fields and velocity dispersion maps of the ionized gas in eight low-z ULIRGs (11 galaxies) covering different phases of the merging process and spanning all levels of activity from pure starbursts to Seyfert nuclei have been investigated using IFS. A comparison of additional available stellar and cold gas kinematic tracers for a sample of 11 ULIRGs (14 galaxies) has also been investigated. The conclusions of this study cover three well-differentiated areas: (1) two-dimensional kinematics of low-z ULIRGs, (2) dynamical mass tracers and their reliability in low-z ULIRGs, and (3) implications for dynamical mass measurements in high-z star-forming galaxies.

The main conclusions regarding the kinematic properties of low-z ULIRGs are as follows:

1. The velocity field of the ionized gas on scales of a few to several kpc does not correspond in general to that of an ordered, inclined, rotating system. On the contrary, large-velocity gradients with peak-to-peak velocity amplitudes of up to 600 km s^{-1} are associated with tidally induced structures such as tidal tails, extranuclear star-forming regions, or the relative velocity of pairs involved in the merger.
2. The velocity dispersion peak of the ionized gas in a large fraction ($\sim$60%) of the ULIRGs studied does not coincide in position with the stellar nucleus as traced by the peak of the near-IR continuum light distribution. The velocity dispersions associated with less massive, secondary nuclei in pairs are not distinguishable from the large-velocity dispersions associated with extranuclear, diffuse ionized gas.
3. The comparison of the stellar and gas kinematic tracers suggests that the cold molecular gas does not share the same velocity field as the stars, and ionized gas and could be more rotationally supported. Data for a larger sample of low-z ULIRGs are needed to confirm this result.

The main conclusions for the different dynamical mass tracers in low-z ULIRGs are as follows:

1. Central ionized gas and stellar velocity amplitudes do generally agree (ratio of 0.92 ± 0.37), although discrepancies exist in some galaxies. On the other hand, the molecular gas shows a central velocity amplitude a factor of 2 (1.9 ± 0.6) larger than that of the stars and ionized gas. The observed velocity amplitudes on scales of several kpc do not trace rotations in general and are therefore not reliable mass estimators of these interacting/merging systems. However, exceptions to this rule like IRAS 17208−0014 do exist.

2. There is a tight correlation between the central ionized gas and stellar velocity dispersions (ratio of 1.01 ± 0.13), while molecular gas velocity dispersions have slightly lower values (average of 0.75 and 0.88 that of the stellar and ionized gas). Therefore, contrary to the central velocity amplitude, the central velocity dispersion is a more robust and homogeneous observable of the internal kinematics and is therefore a more reliable tracer of the dynamical mass in these systems, provided the position of the true nucleus of the galaxy is known through optical or near-IR imaging.

3. The masses derived from the central ionized gas velocity dispersion give an average value of $0.4m_* \pm 0.3m_*$ for the studied sample and confirm previous results that ULIRGs are moderate mass ($\leq m_*$) systems.

The main conclusions regarding the implications for dynamical mass estimates in high-z star-forming systems are as follows:

1. Velocity amplitudes should generally not be used to estimate the dynamical mass of high-z systems, if their stellar structure shows the irregular morphological features characteristic of low-z merging systems like the ULIRGs presented in this study. Likewise, this should be valid for UV and IR-selected systems such as LBGs and SMGs.

2. Central velocity dispersions measured using high equivalent width, optical emission lines should be considered the most reliable, and therefore preferred, tracer of the dynamical mass, provided the location of the nuclear mass concentration is independently established using high angular resolution red or near-IR (rest frame) imaging.

Luis Colina thanks STScI for financial support under the Collaborative Visitors Program. The authors wish to thank the anonymous referee for the detailed and constructive report. We also thank Luis Cuesta for his help in using GRAFICOS. Financial support for this work was provided by the Spanish Ministry for Science and Technology through grant AYA2002-01055. This research has made use of the NASA/IPAC Extragalactic Database (NED), which is operated by the Jet Propulsion Laboratory, California Institute of Technology, under contract with the National Aeronautics and Space Administration.

REFERENCES

Arribas, S., Bushouse, H., Lucas, R. A., Colina, L., & Borne, K. 2004, AJ, 127, 2522
Arribas, S., & Colina, L. 2002, ApJ, 573, 576
———. 2003, ApJ, 591, 791
Arribas, S., Colina, L., & Borne, K. D. 2000, ApJ, 545, 228
Arribas, S., Colina, L., & Clements, D. 2001, ApJ, 560, 160
Arribas, S., et al. 1998, Proc. SPIE, 3355, 821
Barmby, P., et al. 2004, ApJS, 154, 97
Bell, E. F. 2005, in Planets to Cosmology: Essential Science in Hubble's Final Years, ed. M. Livio (Cambridge: Cambridge Univ. Press), in press (astro-ph/0408023)
Bell, E. F., McIntosh, D. H., Katz, N., & Weinberg, M. D. 2003, ApJS, 149, 289
Bender, R., Burstein, D., & Faber, S. M. 1992, ApJ, 399, 462
Blain, A. W., Smail, I. R., Ivison, R. J., Kneib, J. P., & Frayer, D. T. 2002, Phys. Rep., 369, 111
Bushouse, H., et al. 2002, ApJS, 138, 1
Chapman, S. C., Blain, A. W., Ivison, R. J., & Smail, I. R. 2003a, Nature, 422, 695
Chapman, S. C., Windhorst, R., Odewahn, S., Yan, H., & Conselice, C. 2003b, ApJ, 599, 92
Charmandaris, V., et al. 2004, ApJS, 154, 142
Cimatti, A., et al. 2004, Nature, 430, 184
Cole, S., et al. 2001, MNRAS, 326, 255
Colina, L., Arribas, S., & Borne, K. D. 1999, ApJ, 527, L13
Colina, L., Arribas, S., Borne, K. D., & Monreal, A. 2000, ApJ, 533, L9
Colina, L., Arribas, S., & Clements, D. 2004, ApJ, 602, 181
Colina, L., et al. 2001, ApJ, 563, 546
Combes, F., Boissé, P., Mazure, A., & Blanchard, A. 1995, Galaxies and Cosmology (Berlin: Springer)
Conselice, C. J., Bershady, M. A., Dickinson, M., & Papovich, C. 2003, AJ, 126, 1183
Conselice, C. J., Blackburne, J. A., & Papovich, C. 2005, ApJ, 620, 564
Dickinson, M., Papovich, C., Ferguson, H. C., & Budavari, T. 2003, ApJ, 587, 25
Downes, D., & Solomon, P. M. 1998, ApJ, 507, 615
Egami, E., et al. 2004, ApJS, 154, 130
Erb, D. K., et al. 2003, ApJ, 591, 101
———. 2004, ApJ, 612, 122
Evans, A. S., Mazarella, J. M., Surace, J. A., & Sanders, D. B. 2002, ApJ, 580, 749
Farrah, D., et al. 2001, MNRAS, 326, 1333
Förster Schreiber, N. M., et al. 2005, ApJ, in press (astro-ph/0408077)
Franx, M., et al. 2003, ApJ, 587, L79
Frayer, D. T., Reddy, N. A., Armus, L., Blain, A. W., Scoville, N. Z., & Smail, I. 2004, AJ, 127, 728
García-Marín, M., Colina, L., & Arribas, S. 2005 in Starbursts: From 30 Dor to Lyman Break Galaxies, ed. R. de Grijs & R. Gonzalez-Delgado (Cambridge: Cambridge Univ. Press), in press
Genzel, R., Tacconi, L. J., Rigopoulou, D., Lutz, D., & Tecza, M. 2001, ApJ, 563, 527
Genzel, R., et al. 2003, ApJ, 584, 633
Giavalisco, M., Steidel, C. C., & Macchetto, D. 1996, ApJ, 470, 189
Hopkins, A. M. 2004, ApJ, 615, 209
Illingworth, G., & Bouwens, R. 2005, in Penetrating Bars through Masks of Cosmic Dust: The Hubble Tuning Fork Strikes a New Note, ed. D. Block et al. (Dordrecht: Kluwer), in press (astro-ph/0410094)
James, P. A., Bate, C., Wells, M., Wright, G. S., & Doyon, R. 1999, MNRAS, 309, 585
Kobulnicky, H. A., & Gebhardt, K. 2000, AJ, 119, 1608
Le Floch, E., et al. 2004, ApJS, 154, 170
Leitherer, C., et al. 1999, ApJS, 123, 3
Lutz, D., Spoon, H. W. W., Rigopoulou, D., Moorwood, A. F. M., & Genzel, R. 1998, ApJ, 505, L103
Mihos, J. C., & Hernquist, L. 1996, ApJ, 464, 641
Monreal, A. 2004, Ph.D. thesis, La Laguna Univ.
Neri, R., et al. 2003, ApJ, 597, L113
Papovich, C., Dickinson, M., & Ferguson, H. C. 2001, ApJ, 559, 620
Pettini, M., Shapley, A. E., Steidel, C. C., Cuby, J.-G., Dickinson, M., Moorwood, A. F. M., Adelberger, K. L., & Giavalisco, M. 2001, ApJ, 554, 981
Sanders, D. B., & Mirabel, I. F. 1996, ARA&A, 34, 749
Sanders, D. B., Scoville, N. Z., & Soifer, B. T. 1988, ApJ, 335, L1
Scoville, N. Z., et al. 2000, AJ, 119, 991
Shapley, A. E., Erb, D. K., Pettini, M., Steidel, C. C., & Adelberger, K. L. 2004, ApJ, 612, 108
Shapley, A. E., Steidel, C. C., Adelberger, K. L., Dickinson, M., Giavalisco, M., & Pettini, M. 2001, ApJ, 562, 95
Solomon, P. M., Downes, D., Radford, S. J. E., & Barrett, J. W. 1997, ApJ, 478, 144
Spitzer, L. 1987, Dynamical Evolution of Globular Clusters (Princeton: Princeton Univ. Press)
Steidel, C. C., et al. 2004, ApJ, 604, 534
Tacconi, L. J., Genzel, R., Lutz, D., Rogopoulou, D., Baker, A. J., Iserlohe, C., & Tecza, M. 2002, ApJ, 580, 73
Tecza, M., et al. 2004, ApJ, 605, L109
Van Dokkum, P. G., et al. 2004, ApJ, 611,703
Veilleux, S., Kim, D.-C., & Sanders, D. B. 2002, ApJS, 143, 315